Lawrence Berkeley National Laboratory
LBL Publications

Title

Radiation Controllable Synthesis of Robust Covalent Organic Framework Conjugates for Efficient Dynamic Column Extraction of 99TcO4 −

Permalink

https://escholarship.org/uc/item/8kj6g17k

Journal

Chem, 6(10)

ISSN

1925-6981

Authors

Wang, Yue
Xie, Mingshu
Lan, Jianhui
et al.

Publication Date

2020-10-01

DOI

10.1016/j.chempr.2020.08.005

Peer reviewed

eScholarship.org Powered by the California Digital Library
University of California

Radiation controllable synthesis of robust covalent organic framework conjugates for efficient dynamic column extraction of $^{99}TcO_4^-$

Yue Wang[1,2], Mingshu Xie[1], Jianhui Lan[2], Liyong Yuan[2,★], Jipan Yu[2], Jiuqiang Li[1], Jing Peng[1], Zhifang Chai[2], John K. Gibson[3], Maolin Zhai[1,★] and Weiqun Shi[2,4,★]

[1] Beijing National Laboratory for Molecular Sciences, Radiochemistry and Radiation Chemistry Key Laboratory of Fundamental Science, The Key Laboratory of Polymer Chemistry and Physics of the Ministry of Education, College of Chemistry and Molecular Engineering, Peking University, Beijing 100871, China.

[2] Laboratory of Nuclear Energy Chemistry, Institute of High Energy Physics, Chinese Academy of Sciences, Beijing 100049, China. [3] Chemical Sciences Division, Lawrence Berkeley National Laboratory (LBNL), Berkeley, California 94720, USA.

[4] Lead Contact

★ Correspondence: yuanly@ihep.ac.cn (L.Y.)

★ Correspondence: mlzhai@pku.edu.cn (M.Z.)

★ Correspondence: shiwq@ihep.ac.cn (W.S.)

SUMMARY

Anion-scavenging materials tailored for $^{99}TcO_4^-$ trapping are urgently needed for both nuclear related environmental remediation and management of spent nuclear fuel. For the first time, we report here an ultra-robust imidazolium decorated covalent organic framework (COF) conjugate fabricated by an ionizing radiation strategy, for efficient capture of $^{99}TcO_4^-$. The charged imidazolium moieties are controllably anchored into the channel of the COF by simply adjusting the γ-ray dose, thereby leading to tunable ReO_4^- uptake up to 952 mg g^{-1} with high selectivity and fast kinetics. More importantly, the high porosity and ultra-robust nanofiber structure of the COFs make them ideal packing materials for dynamic column experiments. >99.98% ReO_4^-/TcO_4^- can be efficiently separated and re-collected, even after four adsorption-desorption cycles, ranking a new record of the elimination rate for ReO_4^- adsorption. The performance of these materials suggests attractive opportunities in practical applications for TcO_4^- removal from the environment and nuclear waste.

INTRODUCTION

^{99}Tc, the most prevalent isotope of technetium, is a toxic β-emitting radionuclide with a long half-life ($t_{1/2} = 2.1\times10^5$ a)[1]. Due to its high fission yield of 6% in a typical uranium fission reactor, about 2.5 g ^{99}Tc is produced per day in a 100 MW reactor, resulting in high radiation conditions for waste repositories[2]. ^{99}Tc is predominately presented as stable pertechnetate anion, $^{99}TcO_4^-$, which is highly water soluble and can readily migrate into and through the environment[3]. During vitrification of nuclear waste, ^{99}Tc can escape as volatile $^{99}Tc_2O_7$, resulting in low ^{99}Tc loading in the ultimate glass waste form[4]. Moreover, the catalytic redox activity of ^{99}Tc can disrupt control of oxidation states of other key components of spent nuclear fuel[5, 6]. Separation of $^{99}TcO_4^-$ is thus increasingly crucial for spent nuclear fuel reprocessing and environmental contamination remediation.

Since ^{99}Tc is radioactive and cannot be handled in common laboratories, ReO_4^- is often employed as chemical analogue for TcO_4^-. Several approaches have been investigated for TcO_4^-/ReO_4^- removal[7], including reductive immobilization by zero-valent iron (ZVI)[8-10], and direct separation by solvent extraction[11-14] or solid phase adsorption[15-18]. Solid phase adsorption approaches can offer simplicity, reliability, high capacity, low cost, low pollution and regeneration ability. Early efforts towards designing and synthesizing high performance anion-exchange adsorbents for TcO_4^-/ReO_4^- trapping included inorganic cationic framework materials, such as biochar[19], modified Al_2O_3[20], LDHs[21, 22], $Y_2(OH)_5Cl$[23], and NDTB-1[17]. Despite high surface areas, these materials lack specific surface functional groups and thus exhibit low adsorption capacity and poor selectivity. Organic materials including polymeric anion-exchange resins[24-26] and gels[27-29] exhibit efficient uptake of TcO_4^-/ReO_4^- even under acidic conditions, but some of them often suffer from poor radiation resistance[30, 31] and/or slow adsorption kinetics[27]. Cationic metal-organic frameworks (MOFs), self-assembled by metal cations and neutral organic ligands, have become promising candidates for TcO_4^-/ReO_4^- remediation, due to high adsorption capacity, fast kinetics, excellent selectivity, and high radiation stability[32-36]. However, these MOF materials cannot survive highly acidic conditions required for spent nuclear fuel reprocessing, and furthermore do not comply with the CHON principle[37] to avoid secondary contamination caused by metals. More stable and useful adsorbents for efficient TcO_4^-/ReO_4^- capture clearly remain a goal for the sustainable development of nuclear energy.

A new class of porous crystalline materials constructed by strong covalent bond linkages with extended structures, so called covalent organic frameworks (COFs), have increasingly attracted attention[38-41]. Benefitting from structural diversity, permanent porosity and excellent stability, COFs have been developed for many applications[42-48]. When conferred with charged moieties on the skeleton or side chain attachments[49-51], COFs exhibit potential as excellent ion-exchange adsorbents for TcO_4^-/ReO_4^-. COF attributes include the following: (1) Controllable molecular design permits precise integration of functional modules into porous structures, and crystallinity provides high accessibility of functional groups in ordered pores[30, 52, 53]; (2) The local hydrophobic environment in COF pores can enhance selectivity for less hydrophilic TcO_4^-/ReO_4^- over common anions such as NO_3^-, CO_3^{2-}, SO_4^{2-} and PO_4^{3-}; (3) Strong covalent bonds render COFs ultra-robust under harsh chemical conditions[54], and highly conjugated frameworks stabilize radicals generated during the irradiation[30, 31] to mitigate radiation damage; (4) Compared with metal-based materials such as MOFs, COFs are free of metal atoms while only composed of light elements, so secondary pollution caused by metals can be avoided. In other words, COFs comply with the CHON principle, thus can be incinerated completely. Based on these merits, several previous reports have showed brilliant results upon TcO_4^- scavenger by batch experiments[30, 31, 55, 56]. However, if we really expect to put a COF material into practical application, it would be quite necessary to conduct column tests before declaring the success of one applicable adsorbent. Up to now, the dynamic column experiments using COFs to remove ions have never been reported probably due to the high column pressure caused by the very small COF grains[57] and the difficulty in elution. The rational construction of COFs conjugates with suitable structure and porosity is thus a key issue.

On the other hand, introduction of functional groups into COFs can be challenging because chemical functionalities may be incompatible with the COF, and may disrupt COF crystallinity[58]. Post-synthesis COF functionalization by grafting is an appealing alternative synthetic strategy[52, 59-61], among which radiation-induced grafting polymerization represents a typical and mature method of post-synthesis with a long history[62-69]. Compared with chemical initiation, γ-ray radiation-induced grafting possesses advantages of environmentally green, effective, energy efficient and operationally simple for functional modification of substrates. γ-rays are also penetrative enough to ensure the homogeneity of the grafting reaction and thus the excellent mechanical properties of the COFs, which allows continuous and stable operation of the column experiments by maintaining the intrinsic structure of the adsorbent. Again, radiation methods can initiate bulk phase reactions in the absence of initiators, which can reduce impurities in systems. Radiation techniques have been utilized in large scale to easily commercialize the products. The combination of the controllable grafting method and well-defined COFs will definitely achieve truly controllable TcO_4^-/ReO_4^- trapping, yet we are unaware of any results on this topic.

Herein, we present a new strategy to construct cationic COFs for TcO_4^-/ReO_4^- trapping. For the first time, an imidazolium-based ionic liquid, 1-vinyl-3-ethylimidazolium bromide (C_2vimBr), is radiation-induced grafted onto a vinyl-rich COF, designated as TbDa-COF. The resulting modified COF, designated $[C_2\text{vimBr}]_{x\%}$-TbDa-COF where x% is the grafting yield (with detailed definition in supporting information), shown in Figure 1(a), displays rapid adsorption kinetics, high capacity, good selectivity for TcO_4^-/ReO_4^-, and stability under harsh conditions.

More importantly, given the high porosity and ultra-robust nanofiber structure of as-synthesized COF conjugates as well as the very fast adsorption kinetics, dynamic adsorption column experiments based on our COF were successfully conducted, which substantiates the applicability of the COFs for practical TcO_4^-/ReO_4^- trapping. The present results demonstrate that >99.98% ReO_4^-/ TcO_4^- can be efficiently separated and re-collected, even after four adsorption-desorption cycles, recording the elimination rate for ReO_4^- adsorption in literatures. To the best of our knowledge, this is also the first report on dynamic adsorption column experiments based on COFs. The performance of these materials suggests enticing opportunities in practical applications for TcO_4^- removal from the environment, and liquid waste or process streams in spent nuclear fuel reprocessing.

RESULTS AND DISCUSSION

Material design, synthesis and characterization

TbDa-COF was synthesized via imine condensation reaction of 2,5-divinylterephthalaldehyde (DVA) and 1,3,5-tri(4-aminophenyl)benzene (TAPB) (see NMR spectra in Figure S34) in flamed-sealed tubes at 120 °C for 3 days in solvent 1,2-dichlorobenzene/*n*-butylalcohol (*o*-DCB : *n*-BuOH = 1:1) with 9 vol% of 6 M acetic acid as catalyst. Fourier transform infrared (FT-IR) spectra of TbDa-COF show characteristic C=N vibrations around 1608 cm^{-1} [52, 70], and disappearance of the N-H (3355, 3436 cm^{-1}) and aldehydic C-H (2781, 2874 cm^{-1}) modes of the precursors (Figure S1). Besides, the C=C vibration is red-shifted from 1049 cm^{-1} to 1033 cm^{-1}, proving the formation of the conjugated structure. ^{13}C cross-polarization/magic-angle spinning (CP/MAS) NMR spectra confirm C=N bonds at 161 ppm, and disappearance of aldehydic carbon at 186 ppm (Figure S2). Scanning electron and transmission electron microscopy (SEM and TEM) show TbDa-COF morphology of uniform porous nanofibers (Figure 1(b), Figures S3 and S4). Crystallinity of TbDa-COF was verified by powder X-ray diffraction (PXRD) in conjunction with multi-scale computational simulations and Pawley refinement. As shown in Figure 2(a) and Figure S5, TbDa-COF exhibits a strong PXRD peak at 2.98° and weaker peaks at 5.86° and 7.64°, corresponding to the (100), (200) and (210) facets, respectively. The simulations suggest that the AA stacking mode better fits the PXRD pattern than AB stacking (Table S1 and S2). The (001) facet corresponds to a π-π stacking distance of about 3.6 Å along the direction perpendicular to the 2D layers. Porosity of TbDa-COF was determined from nitrogen adsorption-desorption isotherms at 77 K (Figure 2(c)), with the Brunauer–Emmett–Teller (BET) surface area calculated as 1222 $m^2\ g^{-1}$. Nonlocal density functional theory (NLDFT) modeling suggests both micropores and mesopores in TbDa-COF (Figure S6). Besides, the chemical stability of TbDa-COF in various solvents and radiation resistance are demonstrated by the maintenance of its crystallinity (Figure S7(a), Figure S25(a)).

A robust structure and high crystallinity suggested TbDa-COF as a substrate to modify to provide an adsorption material tailored for TcO_4^-/ReO_4^-. Radiation grafting was employed as an effective green method to initiate COF functionalization. The charged moieties of imidazolium-based ionic liquid C_2vimBr were anchored onto the COF channel walls by radical grafting polymerization with the products designated $[C_2vimBr]_{x\%}$-TbDa-COF, where x% is the grafting yield. The influence of absorbed dose and solution concentration of C_2vimBr on grafting yield was assessed using thermogravimetric analysis (TGA) to determine the yield x% in $[C_2vimBr]_{x\%}$-TbDa-COF (Figure 2(f), Figure S8-S10). TGA curves for samples soaked in a solution of 50 wt.% C_2vimBr/MeOH with different exposure times at constant dose rate providing different absorbed doses, exhibit three stages of decomposition (Figure S8): (1) loss of solvent below 200 °C; (2) imidazolium decomposition around 300 °C; and (3) degradation of the COF framework around 450 °C. The weight loss in the second stage provides the grafting yield, which increases with increasing absorbed dose. The calculated grafting yields increase from approximately 28% to 119% upon increasing the absorbed dose from 5 kGy to 40 kGy. The grafting yield also increases with concentration of C_2vimBr for a fixed absorbed dose (Figure S9).

Grafting was confirmed by FT-IR and X-ray photoelectron spectroscopy (XPS) (Figure 2(e) and Figure S11). FT-IR of $[C_2vimBr]_{28\%}$-TbDa-COF exhibits a characteristic imidazolium band at 1167 cm^{-1}, along with disappearance of vinyl bands at 2955 and 1033 cm^{-1}. XPS reveals the Br 3d signal at 67.5 eV for $[C_2vimBr]_{28\%}$-TbDa-COF. In addition, fitting of the N 1s signal indicates imidazolium at 401.7 eV after grafting. PXRD of $[C_2vimBr]_{x\%}$-TbDa-COF shows similar patterns as pristine COF (Figure 2(b)), indicating negligible changes in crystallinity and structure upon radiation-induced grafting. Nitrogen adsorption measurements give a BET surface area of $[C_2vimBr]_{x\%}$-TbDa-COF that continues to decrease as the grafting rate increases (Figure S12) due to the introduction of imidazolium functional groups into the COF pores, but there is still a preservation of porosity after grafting (Figure 2(d) and Figure S13). SEM images of $[C_2vimBr]_{x\%}$-TbDa-COF show uniform nanofibers with rough surfaces (Figures 1(c), 1(d) and Figure S14), demonstrating retention of morphology in the grafted materials. Besides, the chemical stability of the grafted COFs after treatment in various solvents is demonstrated by the maintenance of their crystallinity and morphology (Figure S7(b) and Figure S23(a-c)).

ReO_4^- sorption studies

To access trapping performance for TcO_4^-/ReO_4^-, adsorption kinetics were investigated using $[C_2vimBr]_{24\%}$-TbDa-COF and $[C_2vimBr]_{119\%}$-TbDa-COF as representative of low and high grafting yields. 5 mg of the COF material was added to 10 mL aqueous solution; ReO_4^- concentrations were measured by ICP-AES. As shown in Figure 3(a), Figures S15 and S16, adsorption kinetics depend on both grafting yield and initial Re concentration. For all samples, equilibrium was achieved within 30 min, with $[C_2vimBr]_{24\%}$-TbDa-COF attaining equilibrium in 2 min for initial concentration of 500 ppm Re (rate constant k_2 = 1.05×10^{-2} $g\cdot mg^{-1}\cdot min^{-1}$). The adsorption kinetics is much faster than that of commercial anion-exchange resins such as Purolite A532E and Purolite A530E (~2.5 h)[30], and is comparable to the fastest reported in the literature including those for SCU-COF-1[30], $DhaTG_{Cl}$[55], SCU-CPN-1-Cl[31], PQA-*p*N(Me)$_2$Py-Cl[56] and HPS-P[71]. Such efficient adsorption reflects accessible functional groups in ordered COF pores, an effect that would facilitate rapid sequestration in the event of a radiological release into the environment.

Trapping capacity of $[C_2vimBr]_{x\%}$-TbDa-COF for ReO_4^- was further evaluated by determining equilibrium Re concentrations after exposure to aqueous ReO_4^- solutions at initial concentrations from 25 to 800 ppm. The adsorption isotherm curves in Figure 3(b) give saturated adsorption capacities fitted by the Langmuir model (correlation coefficient 0.99) in the range of 199 to 952 mg ReO_4^- g^{-1} $[C_2vimBr]_{x\%}$-TbDa-COF. For comparison, the adsorption by ungrafted TbDa-COF is fitted by the Freundlich model (Figure S17), with a capacity of only 74 mg ReO_4^- g^{-1}. The maximum saturated adsorption capacity here of 952 mg ReO_4^- g^{-1} (Figure 3(c)) is higher than those of commercial anion-exchange resins such as Purolite A532E (446 mg ReO_4^- g^{-1}) and Purolite A530E (706 mg ReO_4^- g^{-1})[30], and most reported cationic materials (Table S4) including LDHs (130 mg g^{-1})[34], UiO-66-$NH_3^+Cl^-$ (159 mg g^{-1})[72], SCU-101 (217 mg g^{-1})[33], SCU-102 (291 mg g^{-1})[36], PAF-1-F (420 mg g^{-1})[73], $DhaTG_{Cl}$ (437 mg g^{-1})[55], SCU-100 (541 mg g^{-1})[32], SLUG-21 (602 mg g^{-1})[74], SCU-COF-1 (702 mg g^{-1})[30], and SBN (786 mg g^{-1})[34], but is somewhat lower than for SCU-CPN-1 (999 mg g^{-1})[31] and PQA-*p*$N(Me)_2$Py-Cl (1127 mg g^{-1})[56]. Such a high capacity for ReO_4^- sets the grafted COFs as a significant anion-exchange material with one of the highest reported exchange capacities. Besides, to provide a further insight into the effect of grafting on the ReO_4^-/TcO_4^- removal, we have compared the Re uptake by different grafted COFs with respect to the theoretical maximum adsorption capacity, experimental adsorption capacity, and their ratio, as given in Table S5. As can be seen, with the increase of grafting yield, the ratio of experimental capacity to theoretical maximum capacity decreases. This is understandable given that high content of grafted imidazolium causes steric hindrance effect, and prevents ReO_4^- approaching the internal adsorption sites for effective ion exchange, thereby reducing the utilization opportunity of adsorption sites. Overall, control of grafting and resultant adsorption, as demonstrated by the results in Figure 3(c), bodes well for utility of the new COF materials in TcO_4^- removal applications.

Given the presence of various anions in radioactive waste streams, anion exchange selectivity is needed for practical applications of TcO_4^- adsorbents. Therefore, the adsorption properties of $[C_2vimBr]_{24\%}$-TbDa-COF and $[C_2vimBr]_{119\%}$-TbDa-COF for ReO_4^- in the presence of NO_3^-, Cl^-, SO_4^{2-}, CO_3^{2-} and PO_4^{3-} was evaluated (Figure 3(d), Figure S18). With the competing anions at the same concentration as ReO_4^-, the removal percentages remained as high as 92% to 96% for 1 mg adsorbent per mL solution, while the values for all the competing anions were less than 57% (determined by ion chromatography), representing a priority in uptake for ReO_4^-. The selectivity shown here is comparable to that of SCU-COF-1[30], SCU-100[32], and SCU-CPN-1-Cl[31], but much better than most of the reported materials including commercial resins such as A520E and IRA-401[55]. Considering the typical excess of NO_3^- and SO_4^{2-} in certain types of nuclear waste solutions, we also investigated the uptake of ReO_4^- as a function of their concentrations (Figures 3(e), 3(f)), Figures S19, S20). As can be seen, even for concentrations of NO_3^- : ReO_4^- = 100 : 1, and SO_4^{2-} : ReO_4^- = 1000 : 1, the removal of ReO_4^- was still as high as ~50% and ~65%, respectively, which further confirms the high selectivity of the COF adsorbent for ReO_4^-. The high selectivity can be rationalized from the hydrophobic nature of the COF channels constructed by benzene-rich ligands. Specially, ReO_4^- is a large, monovalent anion, thereby resulting in a low charge to radius ratio and an overall low charge density. The standard Gibbs energy of hydration of ReO_4^- (-330 kJ mol^{-1}) is also greatly lower than those of SO_4^{2-} (-1090 kJ mol^{-1}) and PO_4^{3-} (-2773 kJ mol^{-1})[7, 75], which is in favor of its extraction from the water media. In other words, ReO_4^- appears less hydrophilic, which is more favored by the hydrophobic COF channels, thus leading to a better selectivity. Besides, it is worth noting that under the same condition, NO_3^- made the removal percentage of ReO_4^- decrease more than SO_4^{2-}. This phenomenon follows the principle of anti-Hofmeister bias that can also be attributed to the hydrophobic nature of the COF skeleton. NO_3^- with lower charge density possesses a higher affinity with the hydrophobic skeleton to compete with ReO_4^- than SO_4^{2-}, thus gives more negative effect on the removal of ReO_4^-. Overall, it can be concluded that construction of hydrophobic pores in an adsorbent not only improves the selectivity for ReO_4^- but also affects the affinity for those anions with different charge densities.

The adsorption properties and the zeta-potential of the COF adsorbent as a function of pH were also studied in detail, and the results are shown in Figure S21 and Figure S22. As can be seen, the grafted COF shows positive zeta potential in the whole test pH range (3~11), revealing a definite positively charged surface. This guarantees the grafted COF to maintain a good adsorption performance over a wide pH range, which is consistent with the adsorption results of no clear changes in the ReO_4^- uptake at pH 3~9. At pH 1, however, the ReO_4^- uptake is significantly decreased. Since the content of anions in a solution with pH = 1 is approximately 100 times higher than that of ReO_4^-, the decrease in the adsorption capacity is probably due to the competition of anions in the system but not the effect of the hydrogen ions. Stability performance of the grafted COFs in acid and other solvent media was then tested. The grafted COFs maintained their high adsorption capacities for ReO_4^- after being soaked in various media (Figure S24). Combining the adsorption results in Figure S21 and SEM images in Figure S23 (a-c), it can be concluded that the COF material maintains stable in various solvents or aqueous solutions ranging from of 1 M HCl to pH 9.0. To assess the radiation stability of the grafted COFs, dry samples and samples soaked in water were subjected to ^{60}Co gamma irradiation using a dose rate of 160 Gy min^{-1}, up to a maximum dose of 200 kGy. No discernable changes in morphology, PXRD patterns and FTIR spectra (Figures S23(d-g), S25(b), S26) indicate the maintenance of COF framework during the irradiation. And no decrease in Re(VII) adsorption (Figure S27) was observed for all the test samples even following 200 kGy irradiation, which confirms excellent radiation stability. The stability of the COFs can be rationalized from their unique structures involving extended π-conjugation frameworks and close π-π stacking, which has been demonstrated by the previously reported works[30, 58].

Sorption mechanism

The adsorption mechanism of grafted COFs was investigated using various probes. The new FT-IR peak at 908 cm^{-1} in Figure 4(a) after ReO_4^- adsorption corresponds to Re-O stretching vibrations. The FT-IR spectrum after subsequent treatment with 1 M KBr at room temperature indicates near complete elimination of ReO_4^-, confirming an anion exchange mechanism. XPS spectra in Figure 4(b) and Figure S28 show new Re 4f peaks after adsorption, with those due to Br 3d essentially gone. For $[C_2vimBr]_{x\%}$-TbDa-COF with higher grafting yields, residual Br 3d peaks remained, presumably due to internal COF defects such that not all anion-exchange sites are utilized. The N 1s peak at 401.7 eV was essentially unaffected by ReO_4^- adsorption, suggesting little effect of Br^-/ReO_4^- exchange on the imidazolium groups. SEM-EDS and ion chromatography also support the postulated anion exchange mechanism (Figures 1(e), 4(e) and Figure S29). From Figure 4(e) it is apparent that the equilibrium concentration of exchanged-out bromide ions is inversely related to ReO_4^- removal, with the ratio of adsorbed ReO_4^- to released Br^- close to 1:1. Extended X-ray absorption fine structure (EXAFS) spectra in Figure 4(d) show raw and Fourier transformed Re L_{III}-edge k^3 weighted EXAFS spectra for Re(VII)-loaded COF and $KReO_4$; the similar EXAFS spectra and metric parameters (Table S3) indicate essentially the same speciation and coordination structure of Re(VII) upon adsorption, in accord with Re 4f XPS results in Figure 4(c).

We further explored the adsorption dynamics of ReO_4^- anions into the structure of the COF adsorbent and the underlying uptake mechanism using all-atom molecular dynamics (MD) simulations in combination with first principles calculations (see details in the the Supporting Information SI-Computational methods and analysis of ion-exchange process). The comparison of Figure S30 and Figure

S31 clearly shows the occurence with time evolution of the ion exchange between ReO_4^- and Br^- anions. The interaction energies between different components of the simulation system at the last several ns were then analyzed. The binding energy of ReO_4^- with water (-66 kcal/mol) is clearly lower than that of Br^- (-76 kcal/mol), which is well consistent with the reported results[75] that ReO_4^- has a lower hydration energy, thus being in favor of its extraction from water. To uncover the driving forces for the anion-exchange process, density functional theory calculations with the BHLYP functional using Gaussian 16 software were also performed (see details in the Supporting Information SI-Computational methods and analysis of ion-exchange process and Figure S32). The results suggest that compared to Br^-, ReO_4^-/TcO_4^- show slightly larger binding energy by 3.1 kcal/mol with the side chain of the COF. We thus conclude by combining the MD simulations that ReO_4^-/TcO_4^- have slightly higher binding ability with the COF while significantly weaker solvation ability in water than Br^-. That is to say, the less hydrophilic nature of ReO_4^-/TcO_4^- than Br^- dominates the ion exchange process, which is in line with our deduction in the previous section and the conclusion drawn from the recently published works on ReO_4^-/TcO_4^- removal via ion exchange[30, 31, 56].

Dynamic adsorption column experiments for $^{99}TcO_4^-$ remediation

To evaluate dynamic adsorption performance relevant to applications, experiments were performed with grafted COF adsorbents packed into columns, with details in Figure 5(b) and supporting information. Experiments were first conducted with ReO_4^- aqueous solutions using TbDa-COF and $[C_2vimBr]_{16\%}$-TbDa-COF (Figure S33), with complete breakthrough for the latter taking much longer due to enhanced adsorption after grafting. Reusability of $[C_2vimBr]_{16\%}$-TbDa-COF was evaluated using aqueous solutions of 25 ppm Re(VII) for adsorption, and 1 M KBr for elution, which was pumped through the column at a flow rate of 1.0 mL min^{-1}. After complete adsorbent saturation followed by washing with pure water, ReO_4^- was readily desorbed by 20 mL of 1 M KBr and the column was then washed by pure water and recovered for the next of the four cycles (Figure 5(a)). Notably, the results in Figure 5(c) indicate >99.98% adsorption removal of ReO_4^- in all four cycles, with the residual concentration of Re (measured by ICP-MS) decreased to as low as 0.8 ppb. This value is lower than the maximum concentration limit of World Health Organization (WHO) set for heavy metal ion in drinking water. From this point of view, the material reported here and its packed column are effective and feasible for water purification. Furthermore, the result in Figure 5(d) that over 91% ReO_4^- is recovered in desorption stages indicates good recycling efficiency. The high separation efficiency is believed to result from the high porosity and nanofiber structure of the COFs, and anion exchanger present in large quantities in the COFs, whereas the good recycling efficiency can be attributed to the ultra-robust nature of the COFs, and the excellent mechanical properties of the COFs due to radiation-induced homogeneous grafting, as evidenced by the stable column pressure and the maintenance of their morphology (Figure S23(h)) during several column separation cycles.

Finally, we directly demonstrated usability of the $[C_2vimBr]_{16\%}$-TbDa-COF column for TcO_4^- remediation using aqueous solutions of 10 ppm Tc(VII) with the same flow rate of 1.0 mL min^{-1}. In order to reduce the amount of radioactive waste, only 10 mL of Tc solution was fed in the adsorption stage, which was far from saturation. And only 5 mL of 1 M KBr and 5 mL of water were used in the desorption stage where TcO_4^- was stripped from the column into the eluent and then detected by a liquid scintillation counter. As shown in Figure 5(e), in the adsorption stage, TcO_4^- is almost completely immobilized with an adsorption rate of over 99.98%, while in the subsequent desorption stage, the desorption rate is about 70%. This value is lower than that for Re column experiments where the adsorption stage was saturated and 20 mL of 1 M KBr was used for desorption. We believe that if the same procedure as that in

Re column experiments was adopted, a high desorption rate over 90% can be achieved. Overall, these results confirm promise for applications of the grafted COF and its packed column in TcO_4^- removal.

Conclusions

In summary, using radiation-induced grafting we synthesized imidazolium modified 2D COFs $[C_2vimBr]_{x\%}$-TbDa-COF for ReO_4^-/TcO_4^- trapping. As a result of accessible and flexible cationic sites in highly ordered and stable hydrophobic channels, these adsorbents exhibit tunable ReO_4^- adsorption capacities up to 952 mg g^{-1} and unparalleled fast kinetics, with equilibrium in as low as 2 min. The adsorbents retain satisfactory uptake performance for ReO_4^-/TcO_4^- even with large excesses of common competing anions. Dynamic adsorption experiments demonstrated effective trapping of ReO_4^-, recyclability, and applicability to separation of radioactive TcO_4^-. The results reveal enormous potential for spent nuclear fuel reprocessing and environmental remediation, which should motivate further exploration of this family of COF materials.

EXPERIMENTAL PROCEDURES

Resource Availability

Lead Contact

Further information and requests for resources and reagents should be directed to and will be fulfilled by the Lead Contact, Weiqun Shi (shiwq@ihep.ac.cn).

Materials Availability

This study did not generate new unique reagents.

Data and Code Availability

The published article includes all datasets generated or analyzed during this study.

Synthesis, Characterization, Adsorption experiments and Modeling

TbDa-COF was synthesized by TAPB and DVA through vacuum solvothermal reaction. The modified $[C_2vimBr]_{x\%}$-TbDa-COF was synthesized by radiation-induced grafting C_2vimBr onto TbDa-COF. The structure, morphology, porosity and grafting yield of the materials were characterized by FTIR, solid state NMR, XPS, XRD, SEM, TEM, N_2 adsorption, TGA, et al. Batch adsorption experiments were performed by mixing the prepared adsorbents with $KReO_4$ aqueous solution. After shaken at 25 °C at a rate of 180 rpm for the specified contact time, the samples were separated with a 0.22 μm nylon membrane filter, diluted and subjected to ICP-AES for concentration measurement. The adsorption mechanism was illustrated by FTIR, XPS, EXAFS, supplemented by computational simulation. The flow rate of the dynamic adsorption column experiments was 1.0 mL min^{-1}, and the feed solution contains 25 ppm Re(VII) or 10 ppm Tc(VII). Full details can be found in the Supplemental Experimental Procedures.

SUPPLEMENTAL INFORMATION

Supplemental information includes synthetic procedures, characterization data, fitting results of experimental sorption data, modeling details, liquid and solid NMR data and can be found with this article online.

ACKNOWLEDGEMENTS

This work was supported by the National Natural Science Foundation of China (Grants Nos. 21701154, 21777161, 11875078 and 21836001) and the National Science Fund for Distinguished Young Scholars (No. 21925603). The Science Challenge Project (TZ2016004) and Youth Innovation Promotion Association of CAS (21017020) are also acknowledged. The work of J. K. G. was supported by the U.S. Department of Energy, Office of Basic Energy Sciences, Heavy Element Chemistry program at LBNL under Contract No. DE-AC02-05CH11231.

AUTHOR CONTRIBUTIONS

M.Z, W.S. and Z.C. conceived the project. Y.W. and L.Y. designed the experiments. Y.W., M.X. and J.Y. performed the sorption experiments and carried out the structural characterizations. J.L. performed the irradiation experiments. L.Y. and J.L. carried out the DFT calculations and analysis of EXAFS data. J.L. performed the analysis of PXRD diffraction data and refined the PXRD data. Y.W., L.Y., J.P. J.G., M.Z. and W.S. discussed the results and wrote the paper.

DECLARATION OF INTERESTS

The authors declare no competing interests.

Figure 1. **Preparation schematic and electron micrographs of [C$_2$vimBr]$_{x\%}$-TbDa-COF, where x% is the grafting yield. (a)** Synthetic procedures for TbDa-COF and [C$_2$vimBr]$_{x\%}$-TbDa-COF. SEM images of **(b)** TbDa-COF, **(c)** [C$_2$vimBr]$_{28\%}$-TbDa-COF and **(d)** [C$_2$vimBr]$_{119\%}$-TbDa-COF. **(e)** EDS mapping of [C$_2$vimBr]$_{28\%}$-TbDa-COF before (above) and after (below) ReO$_4^-$ adsorption. (scale bar 10 μm)

Figure 2. **COF characterization. (a)** PXRD patterns of TbDa-COF; experimental data in red, Pawley refinement in black, computational simulation in blue, and refinement/experiment difference in olive-green. Inset: AA stacking mode of TbDa-COF with C atoms in purple and N in blue (H omitted for clarity). **(b)** PXRD patterns of TbDa-COF, [C$_2$vimBr]$_{28\%}$-TbDa-COF, [C$_2$vimBr]$_{52\%}$-TbDa-COF and [C$_2$vimBr]$_{94\%}$-TbDa-COF. 77 K N$_2$ adsorption/desorption isotherms of **(c)** TbDa-COF and **(d)** [C$_2$vimBr]$_{28\%}$-TbDa-COF. **(e)** FT-IR spectra of TbDa-COF, [C$_2$vimBr]$_{28\%}$-TbDa-COF and C$_2$vimBr. **(f)** Grafting yield versus absorbed dose.

Figure 3. **ReO$_4^-$ adsorption results.(a)** Adsorption kinetics of ReO$_4^-$ (initially 500 ppm) by [C$_2$vimBr]$_{24\%}$-TbDa-COF. **(b)** Adsorption isotherms of [C$_2$vimBr]$_{x\%}$-TbDa-COF having different x%. **(c)** Saturated adsorption capacity versus grafting yield.**(d)** Effect of competing anions on ReO$_4^-$ removal by [C$_2$vimBr]$_{24\%}$-TbDa-COF. (initially 26 ppm, molar ratio = 1 : 1) **(e)** Effect of NO$_3^-$ on removal of ReO$_4^-$ (initially 26 ppm) by [C$_2$vimBr]$_{24\%}$-TbDa-COF. **(f)** Effect of SO$_4^{2-}$ on removal of ReO$_4^-$ (initially 26 ppm) by [C$_2$vimBr]$_{24\%}$-TbDa-COF.

Figure 4. **Assessing the adsorption mechanism. (a)** FTIR and **(b)** XPS spectra of [C$_2$vimBr]$_{28\%}$-TbDa-COF before and after anion-exchange with ReO$_4^-$, and after ReO$_4^-$ desorption using 1 M KBr. **(c)** Re 4f XPS spectrum for Re(VII)-loaded COF. **(d)** Raw and Fourier transforms of Re L$_{III}$-edge k^3 weighted EXAFS spectra of (A) Re(VII)-loaded COF and (B) KReO$_4$. The best fits are indicated by orange and green traces. **(e)** Dependence of the concentration of removed ReO$_4^-$ (blue) and released Br$^-$ (pink) from [C$_2$vimBr]$_{28\%}$-TbDa-COF on the initial concentration of ReO$_4^-$, with the concentrations of ReO$_4^-$ and Br$^-$ measured by ICP-AES and ion chromatography, respectively.

Figure 5. Dynamic adsorption column experiments. (a) Dynamic elution curve of [C$_2$vimBr]$_{16\%}$-TbDa-COF packed column for ReO$_4^-$ separation, with the concentrations of ReO$_4^-$ measured by ex-situ ICP-AES.**(b)** Photo of the dynamic adsorption experiment. Efficacy of ReO$_4^-$ **(c)** Removal and **(d)** Desorption for each cycle. **(e)** Dynamic elution curve of [C$_2$vimBr]$_{16\%}$-TbDa-COF packed column for TcO$_4^-$ separation. The feed solution was ReO$_4^-$ or TcO$_4^-$ aqueous solutions containing 25 ppm Re or 10 ppm Tc, which was pumped through the column at a flow rate of 1.0 mL min^{-1}.

REFERENCES

1. Darab, J. G. and Smith, P. A. (1996). Chemistry of technetium and rhenium species during low-level radioactive waste vitrification. Chem. Mater. *8*, 1004-1021.

2. Lee, M. S., Um, W., Wang, G. H., Kruger, A. A., Lukens, W. W., Rousseau, R. and Glezakou, V. A. (2016). Impeding ^{99}Tc(IV) mobility in novel waste forms. Nat. Commun. *7*, 12067.

3. Wildung, R. E., Mcfadden, K. M. and Garland, T. R. (1979). Technetium Sources and Behavior in the Environment. J. Environ. Qual. *8*, 156-161.

4. Banerjee, D., Kim, D., Schweiger, M. J., Kruger, A. A. and Thallapally, P. K. (2016). Removal of TcO_4^- ions from solution: materials and future outlook. Chem. Soc. Rev. *45*, 2724-2739.

5. Marchenko, V. I., Dvoeglazov, K. N. and Volk, V. I. (2009). Use of redox reagents for stabilization of Pu and Np valence forms in aqueous reprocessing of spent nuclear fuel: Chemical and technological aspects. Radiochemistry *51*, 329-344.

6. Zhou, X. M., Ye, G. A., Zhang, H., Li, L., Luo, F. X. and Meng, Z. K. (2014). Chemical behavior of neptunium in the presence of technetium in nitric acid media. Radiochim. Acta. *102*, 111-116.

7. Xiao, C. L., Khayambashi, A. and Wang, S. (2019). Separation and Remediation of $^{99}TcO_4^-$ from Aqueous Solutions. Chem. Mater. *31*, 3863-3877.

8. Li, J., Chen, C. L., Zhang, R. and Wang, X. K. (2016). Reductive immobilization of Re(VII) by graphene modified nanoscale zero-valent iron particles using a plasma technique. Sci. China Chem. *59*, 150-158.

9. Sheng, G. D., Tang, Y. N., Linghu, W. S., Wang, L. J., Li, J. X., Li, H., Wang, X. K. and Huang, Y. Y. (2016). Enhanced immobilization of ReO_4^- by nanoscale zerovalent iron supported on layered double hydroxide via an advanced XAFS approach: Implications for TcO_4^- sequestration. Appl. Catal. B-Environ. *192*, 268-276.

10. Lenell, B. A. and Arai, Y. (2017). Perrhenate sorption kinetics in zerovalent iron in high pH and nitrate media. J. Hazard. Mater. *321*, 335-343.

11. Omori, T., Muraoka, Y. and Suganuma, H. (1994). Solvent-Extraction Mechanism of Pertechnetate with Tetraphenylarsonium Chloride. J. Radioan. Nucl. Ch. *178*, 237-243.

12. Omori, T., Miyairi, M. and Suganuma, H. (1997). Effect of 3,5-dichlorophenol on the extraction of technetium complexes with tetraphenylarsonium chloride. J. Radioanal. Nucl. Ch. *224*, 39-43.

13. Kopunec, R. and Abudeab, F. N. (1998). Extraction of pertechnetate by triphenyltin chloride and trioctyltin chloride. J. Radioanal. Nucl. Ch. *228*, 123-129.

14. Sonar, N. L., De, V., Pardeshi, V., Raghvendra, Y., Valsala, T. P., Sonavane, M. S., Kulkarni, Y. and Kanwar, R. (2012). Analysis of ^{99}Tc in the radioactive liquid waste after extraction into suitable solvent. J. Radioanal. Nucl. Ch. *294*, 185-189.

15. Neeway, J. J., Asmussen, R. M., Lawter, A. R., Bowden, M. E., Lukens, W. W., Sarma, D., Riley, B. J., Kanatzidis, M. G. and Qafoku, N. P. (2016). Removal of TcO_4^- from representative nuclear waste streams with layered potassium metal sulfide materials. Chem. Mater. *28*, 3976-3983.

16. Wang, S. A., Alekseev, E. V., Juan, D. W., Casey, W. H., Phillips, B. L., Depmeier, W. and Albrecht-Schmitt, T. E. (2010). NDTB-1: A supertetrahedral cationic framework that removes TcO_4^- from solution. Angew. Chem. Int. Edit. *49*, 1057-1060.

17. Wang, S. A., Yu, P., Purse, B. A., Orta, M. J., Diwu, J., Casey, W. H., Phillips, B. L., Alekseev, E. V., Depmeier, W., Hobbs, D. T., et al. (2012). Selectivity, kinetics, and efficiency of reversible anion exchange with TcO_4^- in a supertetrahedral cationic framework. Adv. Funct. Mater. *22*, 2241-2250.

18. Williams, C. D. and Carbone, P. (2016). Selective removal of technetium from water using graphene oxide membranes. Environ. Sci. Technol. *50*, 3875-3881.

19. Hu, H., Jiang, B. Q., Wu, H. X., Zhang, J. B. and Chen, X. H. (2016). Bamboo (Acidosasa edulis) shoot shell biochar: Its potential isolation and mechanism to perrhenate as a chemical surrogate for pertechnetate. J. Environ. Radioactiv. *165*, 39-46.

20. Mulcahy, F. M., Houalla, M. and Hercules, D. M. (1994). Adsorption of perrhenate on modified aluminas. J. Catal. *148*, 654-659.

21. Gu, P. C., Zhang, S., Li, X., Wang, X. X., Wen, T., Jehan, R., Alsaedi, A., Hayat, T. and Wang, X. K. (2018). Recent advances in layered double hydroxide-based nanomaterials for the removal of radionuclides from aqueous solution. Environ. Pollut. *240*, 493-505.

22. Wang, Y. F. and Gao, H. Z. (2006). Compositional and structural control on anion sorption capability of layered double hydroxides (LDHs). J. Colloid Interf. Sci. *301*, 19-26.

23. McIntyre, L. J., Jackson, L. K. and Fogg, A. M. (2008). $Ln_2(OH)_5NO_3 \cdot xH_2O$ (Ln = Y, Gd-Lu): A novel family of anion exchange intercalation hosts. Chem. Mater. *20*, 335-340.

24. Bonnesen, P. V., Brown, G. M., Alexandratos, S. D., Bavoux, L. B., Presley, D. J., Patel, V., Ober, R. and Moyer, B. A. (2000). Development of bifunctional anion-exchange resins with improved selectivity and sorptive kinetics for pertechnetate: Batch-equilibrium experiments. Environ. Sci. Technol. *34*, 3761-3766.

25. Gu, B. H., Brown, G. M., Bonnesen, P. V., Liang, L. Y., Moyer, B. A., Ober, R. and Alexandratos, S. D. (2000). Development of novel bifunctional anion exchange resins with improved selectivity for pertechnetate sorption from contaminated groundwater. Environ. Sci. Technol. *34*, 1075-1080.

26. Virolainen, S., Laatikainen, M. and Sainio, T. (2015). Ion exchange recovery of rhenium from industrially relevant sulfate solutions: Single column separations and modeling. Hydrometallurgy *158*, 74-82.

27. Han, D., Li, X. X., Cui, Y., Yang, X., Chen, X. B., Xu, L., Peng, J., Li, J. Q. and Zhai, M. L. (2018). Polymeric ionic liquid gels composed of hydrophilic and hydrophobic units for high adsorption selectivity of perrhenate. Rsc Adv. *8*, 9311-9319.

28. Han, D., Li, X. X., Peng, J., Xu, L., Li, J. Q., Li, H. B. and Zhai, M. L. (2016). A new imidazolium-based polymeric ionic liquid gel with high adsorption capacity for perrhenate. Rsc Adv. *6*, 69052-69059.

29. Yan, Y., Yi, M., Zhai, M. L., Ha, H. F., Luo, Z. F. and Xiang, X. Q. (2004). Adsorption of ReO_4^- ions into polyDMAEMA hydrogels prepared by UV-induced polymerization. React. Funct. Polym. *59*, 149-154.

30. He, L., Liu, S., Chen, L., Dai, X., Li, J., Zhang, M., Ma, F., Zhang, C., Yang, Z., Zhou, R., et al. (2019). Mechanism unravelling for ultrafast and selective $^{99}TcO_4^-$ uptake by a radiation-resistant cationic covalent organic framework: A combined radiological experiment and

molecular dynamics simulation study. Chem. Sci. *10*, 4293-4305.

31. Li, J., Dai, X., Zhu, L., Xu, C., Zhang, D., Silver, M. A., Li, P., Chen, L., Li, Y., Zuo, D., et al. (2018). $^{99}TcO_4^-$ remediation by a cationic polymeric network. Nat. Commun. *9*, 3007.

32. Sheng, D. P., Zhu, L., Xu, C., Xiao, C. L., Wang, Y. L., Wang, Y. X., Chen, L. H., Diwu, J., Chen, J., Chai, Z. F., et al. (2017). Efficient and selective uptake of TcO_4^- by a cationic metal-organic framework material with open Ag^+ sites. Environ. Sci. Technol. *51*, 3471-3479.

33. Zhu, L., Sheng, D. P., Xu, C., Dai, X., Silver, M. A., Li, J., Li, P., Wang, Y. X., Wang, Y. L., Chen, L. H., et al. (2017). Identifying the recognition site for selective trapping of $^{99}TcO_4^-$ in a hydrolytically stable and radiation resistant cationic metal-organic framework. J. Am. Chem. Soc. *139*, 14873-14876.

34. Zhu, L., Xiao, C. L., Dai, X., Li, J., Gui, D. X., Sheng, D. P., Chen, L. H., Zhou, R. H., Chai, Z. F., Albrecht-Schmitt, T. E., et al. (2017). Exceptional Perrhenate/Pertechnetate Uptake and Subsequent Immobilization by a Low-Dimensional Cationic Coordination Polymer: Overcoming the Hofmeister Bias Selectivity. Environ. Sci. Tech. Let. *4*, 316-322.

35. Drout, R. J., Otake, K., Howarth, A. J., Islamoglu, T., Zhu, L., Xiao, C. L., Wang, S. and Farha, O. K. (2018). Efficient capture of perrhenate and pertechnetate by a mesoporous Zr metal-organic framework and examination of anion binding motifs. Chem. Mater. *30*, 1277-1284.

36. Sheng, D., Zhu, L., Dai, X., Xu, C., Li, P., Pearce, C., Xiao, C., Chen, J., Zhou, R., Duan, T., et al. (2019). Successful decontamination of $^{99}TcO_4^-$ in groundwater at legacy nuclear sites by a cationic metal-organic framework with hydrophobic pockets. Angew. Chem. Int. Ed. *58*, 4968-4972.

37. Nash, K. L. and Lumetta, G. J. (2011). Advanced separation techniques for nuclear fuel reprocessing and radioactive waste treatment (Woodhead Publishing Limited)

38. Cote, A. P., Benin, A. I., Ockwig, N. W., O'Keeffe, M., Matzger, A. J. and Yaghi, O. M. (2005). Porous, crystalline, covalent organic frameworks. Science *310*, 1166-1170.

39. Segura, J. L., Mancheno, M. J. and Zamora, F. (2016). Covalent organic frameworks based on Schiff-base chemistry: synthesis, properties and potential applications. Chem. Soc. Rev. *45*, 5635-5671.

40. Diercks, C. S. and Yaghi, O. M. (2017). The atom, the molecule, and the covalent organic framework. Science *355*, eaal1585.

41. Ma, T. Q., Kapustin, E. A., Yin, S. X., Liang, L., Zhou, Z. Y., Niu, J., Li, L. H., Wang, Y. Y., Su, J., Li, J., et al. (2018). Single-crystal x-ray diffraction structures of covalent organic frameworks. Science *361*, 48-52.

42. Liu, H. Y., Chu, J., Yin, Z. L., Cai, X., Zhuang, L. and Deng, H. X. (2018). Covalent Organic Frameworks Linked by Amine Bonding for Concerted Electrochemical Reduction of CO_2. Chem *4*, 1696-1709.

43. Matsumoto, M., Valentino, L., Stiehl, G. M., Balch, H. B., Corcos, A. R., Wang, F., Ralph, D. C., Marinas, B. J. and Dichtel, W. R. (2018). Lewis-Acid-Catalyzed Interfacial Polymerization of Covalent Organic Framework Films. Chem *4*, 308-317.

44. Sun, Q., Aguila, B., Perman, J. A., Butts, T., Xiao, F. S. and Ma, S. Q. (2018). Integrating Superwettability within Covalent Organic Frameworks for Functional Coating. Chem *4*, 1726-1739.

45. Jin, E. Q., Lan, Z. A., Jiang, Q. H., Geng, K. Y., Li, G. S., Wang, X. C. and Jiang, D. L. (2019). 2D sp^2 Carbon-Conjugated Covalent Organic Frameworks for Photocatalytic Hydrogen Production from Water. Chem *5*, 1632-1647.

46. Cui, W.-R., Zhang, C.-R., Jiang, W., Li, F.-F., Liang, R.-P., Liu, J. and Qiu, J.-D. (2020). Regenerable and stable sp^2 carbon-conjugated covalent organic frameworks for selective detection and extraction of uranium. Nat. Commun. *11*, 436.

47. Li, Y., Guo, X. H., Li, X. F., Zhang, M. C., Jia, Z. M., Deng, Y., Tian, Y., Li, S. J. and Ma, L. J. (2020). Redox-Active Two-Dimensional Covalent Organic Frameworks (COFs) for Selective Reductive Separation of Valence-Variable, Redox-Sensitive and Long-Lived Radionuclides. Angew. Chem. Int. Ed. *59*, 2-10.

48. Veber, G., Diercks, C. S., Rogers, C., Perkins, W. S., Ciston, J., Lee, K., Llinas, J. P., Liebman-Peláez, A., Zhu, C., Bokor, J., et al. (2020). Reticular Growth of Graphene Nanoribbon 2D Covalent Organic Frameworks. Chem *6*, 1125-1133.

49. Huang, N., Wang, P., Addicoat, M. A., Heine, T. and Jiang, D. L. (2017). Ionic covalent organic frameworks: Design of a charged interface aligned on 1D channel walls and its unusual electrostatic functions. Angew. Chem. Int. Edit. *56*, 4982-4986.

50. Jansone-Popova, S., Moinel, A., Schott, J. A., Mahurin, S. M., Popovs, I., Veith, G. M. and Moyer, B. A. (2018). Guanidinium-based ionic covalent organic framework for rapid and selective removal of toxic Cr(VI) oxoanions from water. Environ. Sci. Technol. *53*, 878-883.

51. Li, Z. L., Li, H., Guan, X. Y., Tang, J. J., Yusran, Y. R., Li, Z., Xue, M., Fang, Q. R., Yan, Y. S., Valtchev, V., et al. (2017). Three-dimensional ionic covalent organic frameworks for rapid, reversible, and selective ion exchange. J. Am. Chem. Soc. *139*, 17771-17774.

52. Sun, Q., Aguila, B., Perman, J., Earl, L. D., Abney, C. W., Cheng, Y. C., Wei, H., Nguyen, N., Wojtas, L. and Ma, S. Q. (2017). Postsynthetically modified covalent organic frameworks for efficient and effective mercury removal. J. Am. Chem. Soc. *139*, 2786-2793.

53. Sun, Q., Aguila, B., Earl, L. D., Abney, C. W., Wojtas, L., Thallapally, P. K. and Ma, S. Q. (2018). Covalent organic frameworks as a decorating platform for utilization and affinity enhancement of chelating sites for radionuclide sequestration. Adv. Mater. *30*, 1705479.

54. Kandambeth, S., Dey, K. and Banerjee, R. (2019). Covalent organic frameworks: Chemistry beyond the structure. J. Am. Chem. Soc. *141*, 1807-1822.

55. Da, H. J., Yang, C. X. and Yan, X. P. (2019). Cationic Covalent Organic Nanosheets for Rapid and Selective Capture of Perrhenate: An Analogue of Radioactive Pertechnetate from Aqueous Solution. Environ. Sci. Technol. *53*, 5212-5220.

56. Sun, Q., Zhu, L., Aguila, B., Thallapally, P. K., Xu, C., Chen, J., Wang, S., Rogers, D. and Ma, S. (2019). Optimizing radionuclide sequestration in anion nanotraps with record pertechnetate sorption. Nat. Commun. *10*, 1646.

57. Huang, J. J., Han, X., Yang, S., Cao, Y. Y., Yuan, C., Liu, Y., Wang, J. G. and Cui, Y. (2019). Microporous 3D Covalent Organic Frameworks for Liquid Chromatographic Separation of Xylene Isomers and Ethylbenzene. J. Am. Chem. Soc. *141*, 8996-9003.

58. Yu, J., Yuan, L., Wang, S., Lan, J., Zheng, L., Xu, C., Chen, J., Wang, L., Huang, Z., Tao, W., et al. (2019). Phosphonate-Decorated Covalent Organic Frameworks for Actinide Extraction: A

Breakthrough Under Highly Acidic Conditions. CCS Chem. *1*, 286-295.

59. Nagai, A., Guo, Z. Q., Feng, X., Jin, S. B., Chen, X., Ding, X. S. and Jiang, D. L. (2011). Pore surface engineering in covalent organic frameworks. Nat. Commun. *2*, 536.

60. Lu, Q. Y., Ma, Y. C., Li, H., Guan, X. Y., Yusran, Y., Xue, M., Fang, Q. R., Yan, Y. S., Qiu, S. L. and Valtchev, V. (2018). Postsynthetic functionalization of three-dimensional covalent organic frameworks for selective extraction of lanthanide ions. Angew. Chem. Int. Ed. *57*, 6042-6048.

61. Zhang, G., Tsujimoto, M., Packwood, D., Duong, N. T., Nishiyama, Y., Kadota, K., Kitagawa, S. and Horike, S. (2018). Construction of a hierarchical architecture of covalent organic frameworks via a postsynthetic approach. J. Am. Chem. Soc. *140*, 2602-2609.

62. Wang, Y. M., Qiu, J. Y., Peng, J., Li, J. Q. and Zhai, M. L. (2017). One-step radiation synthesis of gel polymer electrolytes with high ionic conductivity for lithium-ion batteries. J. Mater. Chem. A *5*, 12393-12399.

63. Lin, T. R., Shi, M. N., Huang, F. R., Peng, J., Bai, Q. W., Li, J. Q. and Zhai, M. L. (2018). One-Pot Synthesis of a Double-Network Hydrogel Electrolyte with Extraordinarily Excellent Mechanical Properties for a Highly Compressible and Bendable Flexible Supercapacitor. ACS Appl. Mater. Interfaces *10*, 29684-29693.

64. Ni, D. L., Ferreira, C. A., Barnhart, T. E., Quach, V., Yu, B., Jiang, D. W., Wei, W. J., Liu, H. S., Engle, J. W., Hu, P., et al. (2018). Magnetic Targeting of Nanotheranostics Enhances Cerenkov Radiation-Induced Photodynamic Therapy. J. Am. Chem. Soc. *140*, 14971-14979.

65. Ponce-Gonzalez, J., Ouachan, I., Varcoe, J. R. and Whelligan, D. K. (2018). Radiation-induced grafting of a butyl-spacer styrenic monomer onto ETFE: the synthesis of the most alkali stable radiation-grafted anion-exchange membrane to date. J. Mater. Chem. A *6*, 823-827.

66. Wang, Y. M., Huang, F. R., Chen, X. B., Wang, X. W., Zhang, W. B., Peng, J., Li, J. Q. and Zhai, M. L. (2018). Stretchable, Conductive, and Self-Healing Hydrogel with Super Metal Adhesion. Chem. Mater. *30*, 4289-4297.

67. Zhao, N., Peng, J., Liu, G., Zhang, Y. W., Lei, W. Y., Yin, Z. B., Li, J. Q. and Zhai, M. L. (2018). PVP-capped CdS nanopopcorns with type-II homojunctions for highly efficient visible-light-driven organic pollutant degradation and hydrogen evolution. J. Mater. Chem. A *6*, 18458-18468.

68. Chen, G., Wang, Y., Weng, H. Q., Wu, Z. H., He, K. B., Zhang, P., Guo, Z. F. and Lin, M. Z. (2019). Selective Separation of Pd(II) on Pyridine-Functionalized Graphene Oxide Prepared by Radiation-Induced Simultaneous Grafting Polymerization and Reduction. ACS Appl. Mater. Interfaces *11*, 24560-24570.

69. Zheng, X., Ding, X. J., Guan, J. P., Gu, Y., Su, Z. K., Zhao, Y. M., Tu, Y. F., Li, X. H., Li, Y. J. and Li, J. Y. (2019). Ionic Liquid-Grafted Polyamide 6 by Radiation-Induced Grafting: New Strategy To Prepare Covalently Bonded Ion-Containing Polymers and their Application as Functional Fibers. ACS Appl. Mater. Interfaces *11*, 5462-5475.

70. Uribe-Romo, F. J., Hunt, J. R., Furukawa, H., Klock, C., O'Keeffe, M. and Yaghi, O. M. (2009). A crystalline imine-linked 3-D porous covalent organic framework. J. Am. Chem. Soc. *131*, 4570-4571.

71. Li, X. X., Hang, D., Guo, T. T., Peng, J., Xu, L. and Zhai, M. L. (2018). Quaternary phosphonium modified hierarchically macro/mesoporous silica for fast removal of perrhenate. Ind. Eng. Chem. Res. *57*, 13511-13518.

72. Banerjee, D., Xu, W. Q., Nie, Z. M., Johnson, L. E. V., Coghlan, C., Sushko, M. L., Kim, D., Schweiger, M. J., Kruger, A. A., Doonan, C. J., et al. (2016). Zirconium-based metal-organic framework for removal of perrhenate from water. Inorg. Chem. *55*, 8241-8243.

73. Banerjee, D., Elsaidi, S. K., Aguila, B., Li, B. Y., Kim, D., Schweiger, M. J., Kruger, A. A., Doonan, C. J., Ma, S. Q. and Thallapally, P. K. (2016). Removal of Pertechnetate-Related Oxyanions from Solution Using Functionalized Hierarchical Porous Frameworks. Chem.-Eur. J. *22*, 17581-17584.

74. Fei, H. H., Bresler, M. R. and Oliver, S. R. J. (2011). A new paradigm for anion trapping in high capacity and selectivity: Crystal-to-crystal transformation of cationic materials. J. Am. Chem. Soc. *133*, 11110-11113.

75. Dickson, J. O., Harsh, J. B., Lukens, W. W. and Pierce, E. M. (2015). Perrhenate incorporation into binary mixed sodalites: The role of anion size and implications for technetium-99 sequestration. Chem. Geol. *395*, 138-143.

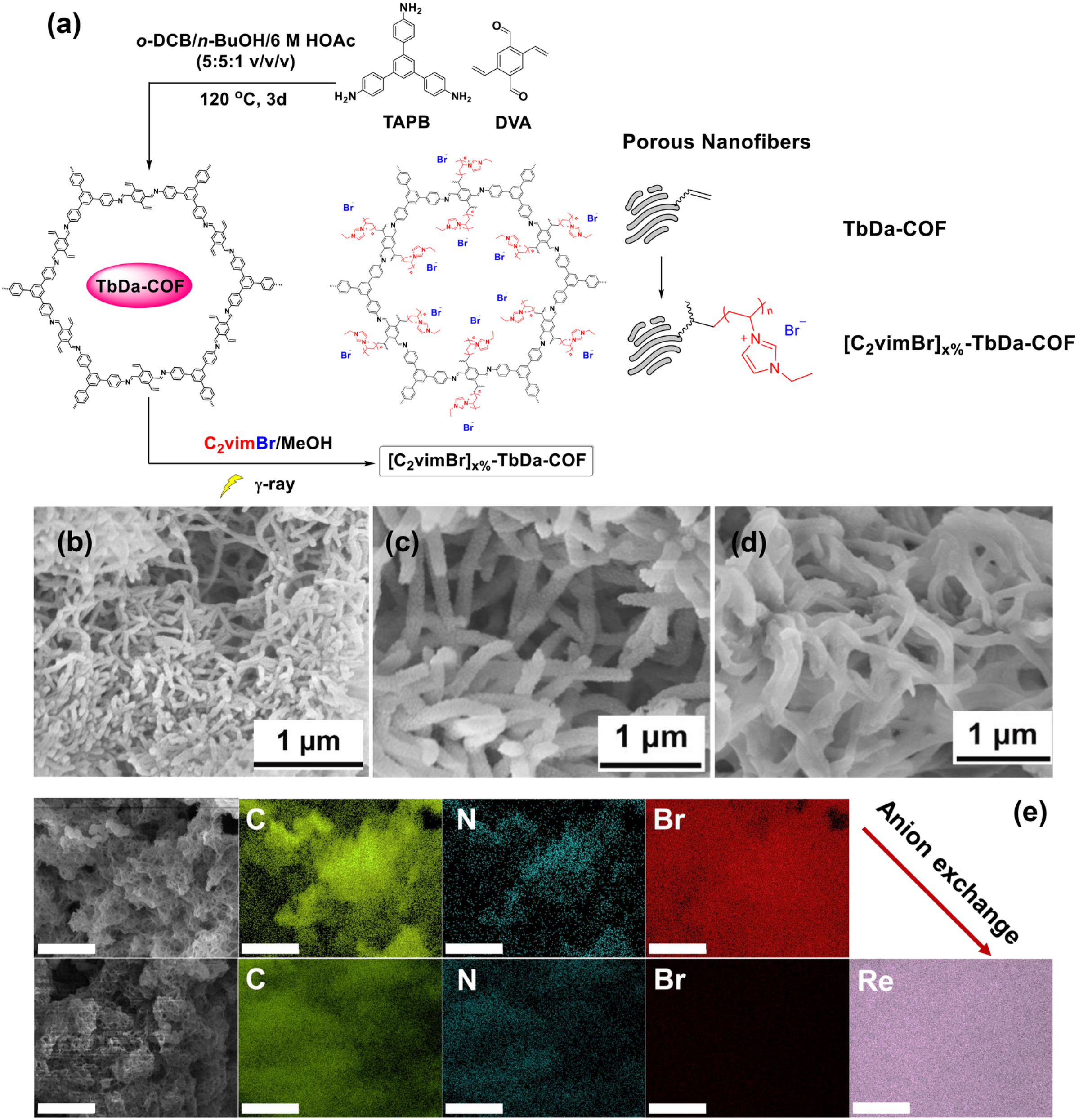
(a)
o-DCB/n-BuOH/6 M HOAc
(5:5:1 v/v/v)
120 °C, 3d
TAPB
DVA
TbDa-COF
C2vimBr/MeOH
γ-ray
[C2vimBr]x%-TbDa-COF
Porous Nanofibers
TbDa-COF
[C2vimBr]x%-TbDa-COF
Br⁻
(b)
1 μm
(c)
1 μm
(d)
1 μm
C
N
Br
(e)
Anion exchange
C
N
Br
Re

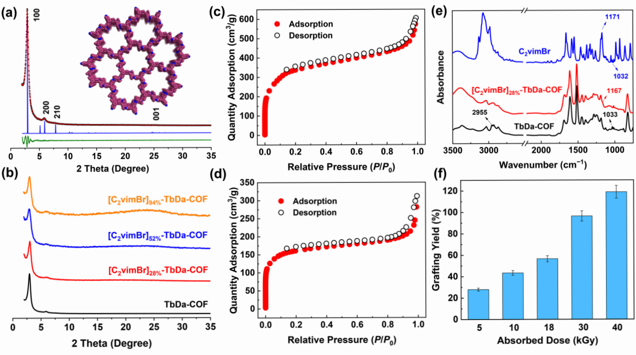
(a)
100
200
210
001
2 Theta (Degree)
(b)
$[C_2vimBr]_{94\%}$-TbDa-COF
$[C_2vimBr]_{52\%}$-TbDa-COF
$[C_2vimBr]_{28\%}$-TbDa-COF
TbDa-COF
2 Theta (Degree)
(c)
Adsorption
Desorption
Quantity Adsorption (cm^3/g)
Relative Pressure (P/P_0)
(d)
Adsorption
Desorption
Quantity Adsorption (cm^3/g)
Relative Pressure (P/P_0)
(e)
C_2vimBr
1171
1032
$[C_2vimBr]_{28\%}$-TbDa-COF
1167
2955
1033
TbDa-COF
Absorbance
Wavenumber (cm^{-1})
(f)
Grafting Yield (%)
Absorbed Dose (kGy)
5
10
18
30
40

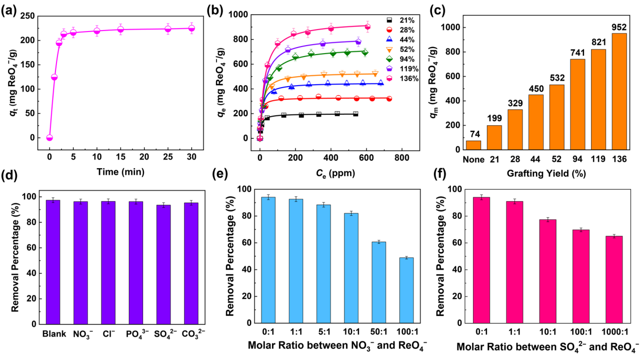
(a)
250
200
150
100
50
0
q_t (mg ReO_4^-/g)
0
5
10
15
20
25
30
Time (min)
(b)
1000
800
600
400
200
0
q_e (mg ReO_4^-/g)
0
200
400
600
800
C_e (ppm)
21%
28%
44%
52%
94%
119%
136%
(c)
1000
800
600
400
200
0
q_m (mg ReO_4^-/g)
74
199
329
450
532
741
821
952
None
21
28
44
52
94
119
136
Grafting Yield (%)
(d)
100
80
60
40
20
0
Removal Percentage (%)
Blank
NO_3^-
Cl^-
PO_4^{3-}
SO_4^{2-}
CO_3^{2-}
(e)
100
80
60
40
20
0
Removal Percentage (%)
0:1
1:1
5:1
10:1
50:1
100:1
Molar Ratio between NO_3^- and ReO_4^-
(f)
100
80
60
40
20
0
Removal Percentage (%)
0:1
1:1
10:1
100:1
1000:1
Molar Ratio between SO_4^{2-} and ReO_4^-

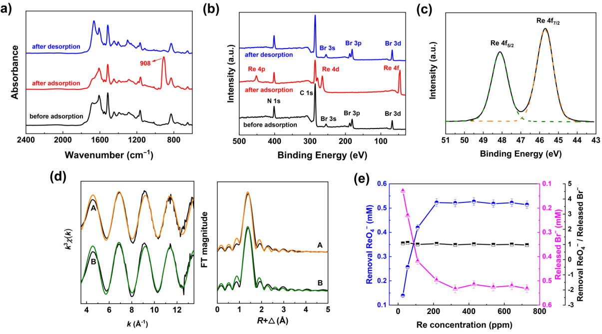
(a)
Absorbance
after desorption
after adsorption
908
before adsorption
2400
2000
1600
1200
800
Wavenumber (cm^{-1})
(b)
Intensity (a.u.)
after desorption
Br 3s
Br 3p
Br 3d
Re 4p
Re 4d
Re 4f
after adsorption
N 1s
C 1s
Br 3s
Br 3p
Br 3d
before adsorption
500
400
300
200
100
Binding Energy (eV)
(c)
Intensity (a.u.)
Re 4f$_{5/2}$
Re 4f$_{7/2}$
51
50
49
48
47
46
45
44
43
Binding Energy (eV)
(d)
$k^3\chi(k)$
A
B
4
6
8
10
12
k (Å^{-1})
FT magnitude
A
B
0
1
2
3
4
5
$R+\Delta$ (Å)
(e)
Removal ReO$_4^-$ (mM)
0.1
0.2
0.3
0.4
0.5
0.6
Released Br$^-$ (mM)
0.1
0.2
0.3
0.4
0.5
0.6
Removal ReO$_4^-$ / Released Br$^-$
5
4
3
2
1
0
-1
-2
-3
0
200
400
600
800
Re concentration (ppm)

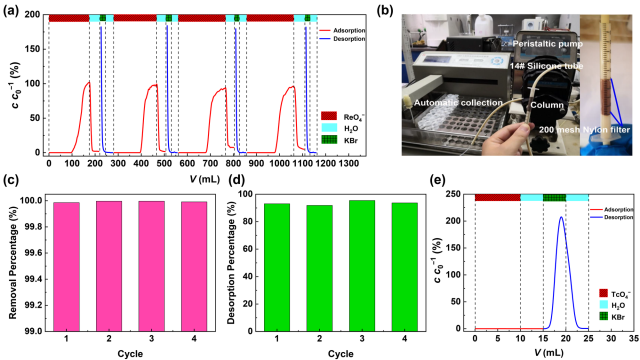
(a)
200
150
100
50
0
$c\,c_0^{-1}$ (%)
0 100 200 300 400 500 600 700 800 900 1000 1100 1200 1300
V (mL)
Adsorption
Desorption
ReO_4^-
H_2O
KBr
(b)
Peristaltic pump
14# Silicone tube
Automatic collection
Column
200 mesh Nylon filter
(c)
Removal Percentage (%)
100.0
99.8
99.6
99.4
99.2
99.0
1 2 3 4
Cycle
(d)
Desorption Percentage (%)
100
80
60
40
20
0
1 2 3 4
Cycle
(e)
250
200
150
100
50
0
$c\,c_0^{-1}$ (%)
0 5 10 15 20 25 30 35
V (mL)
Adsorption
Desorption
TcO_4^-
H_2O
KBr

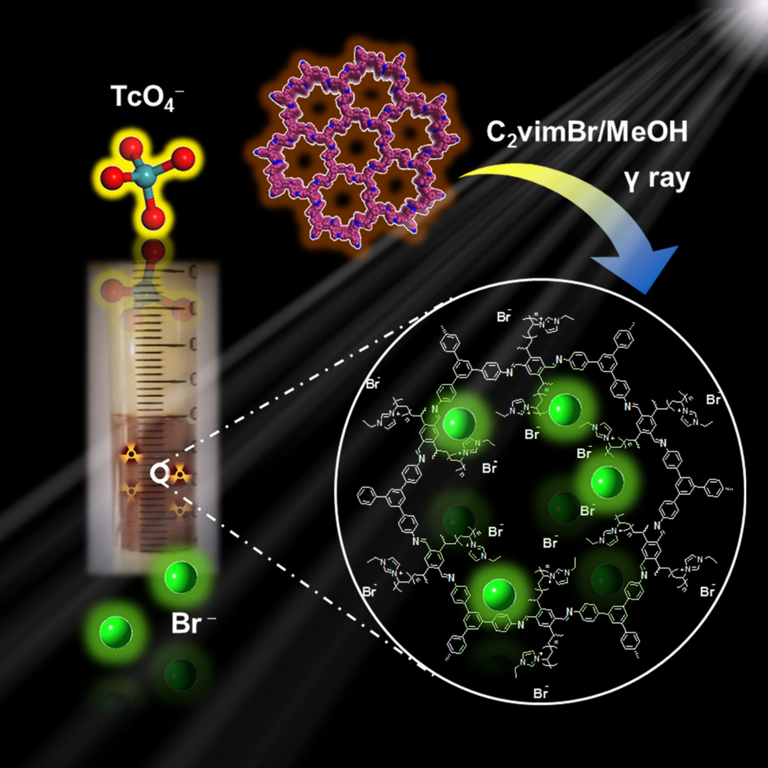
TcO_4^-
$C_2vimBr/MeOH$
γ ray
Br^-